TRENDS IN SCIENCES 2025; 22(7): 9959
https://doi.org/10.48048/tis.2025.9959 RESEARCH ARTICLE

Modification and Enhancement of The Structural, Morphological and Optical Characteristics of PMMA/In_2O_3/SiO_2 Promising Ternary Nanostructures for Optical Nanodevices and Gamma Ray Attenuation

Noor Ali Sami[1], Ayad Mohammed Nattah[2], Rafal A. Jawad[3], Mohanad H. Meteab[4,*] and Musaab Khudhur Mohammed[1]

[1]*Department of Physics, College of Education for Pure Sciences, University of Babylon, Babylon 51002, Iraq*
[2]*College of Materials Engineering, University of Babylon, Babylon 51002, Iraq*
[3]*Department of Physics, College of Sciences, University of Babylon, Babylon 51002, Iraq*
[4]*General Directorate of Education in Babylon Governorate, Ministry of Education, Babylon 51001, Iraq*

([*]Corresponding author's e-mail: mohanad.h.meteab87@gmail.com)

Received: 8 February 2025, Revised: 12 March 2025, Accepted: 7 April 2025, Published: 30 May 2025

Abstract

This study explores the development of poly(methyl methacrylate) (PMMA) composites embedded with varying concentrations (0, 1, 3, and 5 wt.%) of Indium Oxide (In_2O_3) and Silicon Dioxide (SiO_2) through the solution casting technique. X-ray diffraction (XRD) examination established the amorphous nature of pristine PMMA, which evolved into a polycrystalline structure as the additive concentration increased to 5 wt.%. Structural characteristics were further investigated using Fourier Transform Infrared Spectroscopy (FTIR), revealing physical interactions between the polymer matrix and the incorporated nanoparticles. Field Emission Scanning Electron Microscopy (FESEM) demonstrated uniform dispersion of In_2O_3/SiO_2 within the PMMA framework. Optical studies indicated that higher nanoparticle loadings enhanced absorbance, the absorption coefficient, refractive index, extinction coefficient, and both real and imaginary components of the dielectric constant, whereas transmittance and the indirect energy bandgap decreased. The absorption coefficient remained below 10^4 cm^{-1}, confirmatory an indirect electronic transition. Additionally, the gamma-ray attenuation coefficients increased as nanoparticle content rose, suggesting that the (PMMA/In_2O_3/SiO_2) nanocomposites exhibit notable radiation shielding capabilities. These remarkable findings introduced promising materials for optoelectronic and ray attenuation applications. Polymers' transparency, flexibility, and simplicity of fabrication render them ideal for optical nanodevices. Nevertheless, they exhibit inadequate gamma-ray attenuation in comparison to other materials (glass, metal oxides, lead-based materials), which are more effective for gamma-ray shielding. These latter materials are heavier, less malleable, and may be associated with toxicity.

Keywords: In_2O_3, SiO_2, PMMA composite, Nanostructures, Optical characteristics, Gamma radiation

Introduction

The development of effective shielding materials for a variety of applications, such as medical, industrial, nuclear, and space technologies, is essential due to the fact that gamma radiation is a high-energy electromagnetic wave that can penetrate most materials. Dense materials, including lead (Pb), tungsten (W), and concrete, have been traditionally employed for gamma-ray shielding due to their superior radiation attenuation properties and high atomic number (Z) [1-3]. Nevertheless, these materials are heavy, toxic, and difficult to process, which has led to the pursuit of environmentally responsible, lightweight, and more flexible alternatives. Polymer composites have emerged as promising candidates for gamma-ray shielding due to their easy fabrication, low weight, and capacity to incorporate high-Z additives to enhance attenuation

efficiency [2]. Polymer matrices, such as polymethyl methacrylate (PMMA), polyethylene (PE), and epoxy resins, are frequently employed. To improve their shielding abilities, these matrices can be reinforced with metal oxides (e.g., Bi_2O_3, WO_3, In_2O_3), boron-based materials, or nanostructured additives [3]. Polymer nanocomposites represent a class of advanced materials in which polymers enhanced by incorporating nanoscale fillers that exhibit diverse geometries, such as platelets, fibers, spheroids, and other morphologies. These fillers, defined by having at least 1 dimension below 100 nm, play a critical role in modifying and improving the physical, chemical, and mechanical properties of the polymer matrix [4]. The synergistic interaction between the polymer matrix and nanoscale fillers gives rise to novel characteristics often unattainable in conventional composite materials. As a result, nanocomposites demonstrate exceptional properties, including high mechanical strength, thermal stability, electrical conductivity, and barrier performance. These unique attributes make them increasingly valuable in applications such as packaging, electronics, medical implant batteries, and environmental remediation. With their versatility and the ability to integrate multifunctional properties, nanocomposites garnered considerable attention in recent years. Ongoing research continues to focus on developing innovative synthesis and characterization methods to optimize the performance of polymer nanocomposites in advancing modern material science and technology [5].

Poly(methacrylates) are esters of methacrylic acid with the chemical formula $(C_5H_8O_2)_n$ [4]. Among these, poly(methyl methacrylate) (PMMA) is the most widely used. PMMA is a well-established polymer with a long history of applications [5,6]. It is neutral, translucent, and has a density of 1.15 - 1.19 g/cm³ [7]. PMMA is a type of polymer with potential applications as a structural material in orthopedics and orthodontics. Other polymers used for similar purposes include polyethylene and polyether ether ketone (PEEK). While poly(methacrylate) often exhibits lower mechanical strength compared to these alternatives, its superior flexibility in many scenarios compensates for this limitation [8-10]. Due to its cost-effectiveness, chemical and photochemical stability, and excellent light transmission in the visible spectrum, PMMA has become the most successful polymer for disposable contact lenses [11,12]. Additionally, PMMA is widely used in biomedical applications owing to its non-toxicity, chemical stability, and mechanical properties. Even if it doesn't hold up well in shape, PMMA is medically inert and doesn't injure Although it may lack shape retention, PMMA is biocompatible and does not damage tissues [13]. Metal oxide nanoparticles, known for their unique properties, are increasingly employed in medical research and scientific studies. Their intriguing characteristics and superior advantages over bulk materials make them highly valuable in these fields [14]. Indium oxide (In_2O_3) is an n-type semiconductor with a wide bandgap. Semiconductors have garnered significant attention due to their intriguing material properties, including a broad energy bandgap ranging from 3.4 to 3.7 eV [15]. Under stoichiometric conditions, In_2O_3 often exhibits properties. However, in its non-stoichiometric form, it transitions into a semiconductor state characterized by substantial conductivity [16]. In_2O_3 is also recognized as a transparent conducting oxide (TCO), which has attracted considerable interest due to its high electron mobility and low effective electron mass. These remarkable properties have enabled a growing range of applications, including in the production of solar cells Liu [17], antimicrobial treatments Mcieab *et al.* [18], and sensors [19].

Silicon dioxide (SiO_2), also known as silica, naturally occurs as quartz. While all forms of silica share the same chemical composition, their atomic arrangements differ. Silica particles are capable of becoming airborne, forming non-explosive dust [20]. SiO_2 particles enhance the chemical and mechanical properties of materials, acting as effective solid plasticizers. Silica is a fine white powder characterized by excellent thermal stability, mechanical strength, and a high specific surface area. To minimize particle aggregation, silica nanoparticles are often incorporated into polymer matrices using ultrasonic waves [21]. This process enables the production of polymer nanocomposites compatible with polymer electronics. Most Research on SiO_2-infused polymer matrices has predominantly focused on thermal, dielectric, and mechanical properties Mallkpour and Khani [22] However, studies on the linear optical properties of polymer composites containing SiO_2 are relatively scarce [23]. Fumed silica (SiO_2) nanoparticles are

widely employed in industry as nanofillers for electronic packaging and thermoplastic polymers. SiO_2 is an amorphous, non-toxic material that can be integrated into polymer matrices containing nanopores, resulting in nanocomposites suitable for optoelectronic applications [24].

The optoelectronic performance of polymer-based materials, such as PMMA composites, is characterized by their high transparency, tunable refractive index, and excellent optical flexibility, rendering them suitable for optical and electronic applications. Conversely, other conventional materials, including glass, metal oxides, and ceramics, frequently possess higher refractive indices; however, their rigidity and weight restrict their incorporation into lightweight and flexible devices. Compared to denser conventional materials, polymer-based materials are advantageous due to their lightweight nature, which facilitates their integration into sophisticated optoelectronic devices [25].

Polymer materials typically exhibit low intrinsic attenuation for gamma rays as a result of their low atomic number (Z). However, this constraint can be circumvented by incorporating high-Z additives, such as SiO_2 and In_2O_3, which improve the composite's shielding capabilities. In contrast, conventional materials, such as lead-based shielding materials, exhibit exceptional attenuation as a result of their high density and atomic number. Nevertheless, they are less suitable for portable and flexible applications due to their exorbitant weight, environmental hazards, and toxicity. Polymer-based composites are simple to process, cost-effective, and scalable for large-scale production from a fabrication and scalability perspective. At the same time, traditional materials are more expensive and necessitate complex fabrication techniques. Twenty-Medical radiation protection is the most prevalent application of polymer composites in their optoelectronic and ray attenuation applications. Polymer composites are employed to provide lightweight radiation shielding. Gamma-ray shielding for the benefit of astronauts and the materials of spacecraft. Material components for photonic devices, including optical fibers, solar cells, and LEDs [26].

This research centers on the synthesis of PMMA/In_2O_3-SiO_2 nanostructures, integrating PMMA with In_2O_3 and SiO_2 to formulate a novel composite material with superior characteristics, specifically for gamma-ray attenuation and optoelectronic usage. This composite material presents numerous significant advancements compared to conventional materials employed in analogous situations.

Materials and methods

Nanocomposites are composite materials including 2 or more components, with at least one being a nanomaterial. Nanocomposite materials are produced by incorporating a reinforcing phase within a matrix phase. Any phase may constitute the nanomaterial. Consequently, the preparation of PMMA/In_2O_3/SiO_2 nanocomposites, 1 g of PMMA (Alpha Chemika, India), with an average molecular weight of 120,000 g/mol, was dissolved in 50 mL chloroform. The dissolution process involved stirring at ambient temperature for 30 min, followed by an additional 10 min at 70 - 80 °C using a magnetic stirrer to ensure complete dissolution. The resulting solution was poured into sterile Petri dishes and left to dry at room temperature for 24 h, allowing complete solvent evaporation.

PMMA films incorporating indium oxide nanoparticles (In_2O_3 NPs) from Sigma Aldrich (purity 99.8 %, average particle size 30 nm) and silicon dioxide nanoparticles (SiO_2 NPs) from Sigma Aldrich (purity 99.5 %, average particle size 40 nm) were synthesized using the same methodology with adding the ratio dopant for the 0, 0.01, 0.03 and 0.05 for each In_2O_3 and SiO_2 nanoparticles to the PMMA solvent that are summarized in **Table 1**.

The average film thickness was approximately 13 μm. The structure has been determined by X-ray diffractometer (XRD) using (Rigaku-binary (RAW), Ultima Iv, Japan) (Target Cu Kα1 radiation of 1.54060 Å, Current = 30 mA, Voltage = 40 kV, Step = 0.08 deg., scanning speed= 0.25 deg/min., and measurement temperature 25 °C). X-ray diffraction was examined at university of Tehran. The chemical composition of the films was analyzed using Fourier transform infrared spectroscopy (FTIR) (Bruker, model Vertex 70, Germany) at ambient temperature, covering a spectral range of 4000 - 400 cm^{-1}. Surface morphology was examined with a Field Emission Scanning Electron Microscope (FESEM, INSPECT S50, produced by FEI, Japan).

The optical characteristics of PMMA/In_2O_3/SiO_2 nanocomposites were studied using a Shimadzu UV-1650/PC spectrophotometer (Phillips, Japan) across wavelengths ranging from 200 to 800 nm. A sample 1 × 1 cm was taken to test each technique.

Table 1 Summarized the purification of pure PMMA and nanocomposite films.

In_2O_3/SiO_2 (wt.%)	**PMMA (g)**	**In_2O_3 (g)**	**SiO_2 (g)**
0	1	0	0
1	0.99	0.005	0.005
3	0.97	0.015	0.015
5	0.95	0.025	0.025

Results and discussion

The XRD patterns were employed to elucidate the crystallographic structure of PMMA polymer and its nanocomposite films. The nanocomposites contained varying ratios of In_2O_3 and SiO_2 nanoparticles, specifically at 1, 3, and 5 weight percent. This analysis aimed to characterize the structural properties of the nanocomposites at ambient temperature, as illustrated in **Figure 1**. The results indicate that pure PMMA exhibits broad diffraction peaks at 2θ = 15.12° (strong) and 30.19°, reflecting its amorphous characteristics [27]. This indicates the absence of chemical bonds between PMMA and In_2O_3 and SiO_2 nanoparticles. Similarly, the PMMA/In_2O_3/SiO_2 nanocomposites with low nanoparticle content displayed broad and subdued peaks, comparable to pure PMMA, suggesting no chemical bonding between PMMA and the nanoparticles. However, nanocomposites with higher nanoparticle loading (5 wt.%) exhibited distinct XRD peaks at 31.64, 45.44, 53.54, and 56.34°, corresponding to the Miller indices (222), (431), (440), and (611) respectively. These peaks align with the characteristic diffraction of In_2O_3 nanoparticles (JCPDS 06-0416), that match with data reference Anshu S. et. al. that found the peaks at 2θ = 30.77, 45.89, 51.25 and 56.24° correspond to the (222), (431), (440) and planes of the cubic bixbyite In_2O_3 [28]. The XRD patterns further validated the amorphous characteristics of SiO_2, indicated by a large peak at 14.09°, which is masked by the extensive diffraction band of PMMA. No further diffraction peaks were detected, hence affirming the lack of contaminants in the SiO_2 nanoparticles, as corroborated by the JCPDS file for SiO_2 [29].

Analysis of the nanocomposite patterns reveals that the reveals that incorporating 5 wt.% of In_2O_3 and SiO_2 nanoparticles significantly influenced the structural properties of PMMA. This transformation is attributed to interactions between In_2O_3 and SiO_2 nanoparticles, which, convert the amorphous nature of pure PMMA into a polycrystalline structure.

The freshly synthesized pure PMMA and PMMA/In_2O_3/SiO_2 nanocomposite were characterized by FTIR spectroscopy. **Figure 2** presents the FTIR spectra of pure PMMA in image (A) and those of PMMA with different concentrations of In_2O_3/SiO_2 nanoparticles (NPs) in images (B, C, and D), spanning the range of 4000 - 400 cm^{-1}. The absorption band of PMMA, shown in **Figure 2 (A)**, appears at 3018.05 cm^{-1} and corresponds to the asymmetric stretching vibrations of CH_3 groups. The band at 1728.83 cm^{-1} is attributed to the C=C stretching vibration, while the band at 1214.48 cm^{-1} is associated with the C–C–O bond. The bands at 744.03 and 667.52 cm^{-1} are assigned to the C=C stretch and the in-plane deformation vibrations (CCO bending), respectively [30,31]. The addition of In_2O_3 and SiO_2 nanoparticles to the PMMA polymer at varying concentrations (1, 3, and 5 wt.%) resulted in changes to the intensities of specific bands and variations in others, as illustrated in images B and C. The data suggests that the introduction of In_2O_3 and SiO_2 nanoparticles led to a physical interaction with the polymer matrix. In other PMMA-based nanocomposites, such as PMMA/CuO, nanoparticles influence the polymer's vibrational modes and cause alterations in characteristic absorption peaks, which is in accordance with the results of prior research [32].

The arrangement of In_2O_3 and SiO_2 nanoparticles within the PMMA polymer was examined using a field emission electron microscope (FESEM), followed by an assessment of their impact on the nanocomposites. The FESEM images of the (PMMA/In_2O_3/SiO_2) nanocomposites are presented in **Figure 3**. The data shown in (A) indicate that the polymer exhibits cohesiveness and homogeneity. The incorporation of In_2O_3 and SiO_2 nanoparticles into the PMMA polymer alters the surface structure, the arrangement, as shown in images B, C, and E. loading levels, the nanoparticles are uniformly distributed within the polymer matrix. However, at higher concentrations (5 wt.%), they tend to aggregate, forming clusters. This phenomenon may be attributed to the connections between the In_2O_3 and SiO_2 nanoparticles and the PMMA polymer matrix, as confirmed by XRD analysis. These findings are consistent with previous research conclusions [33,34].

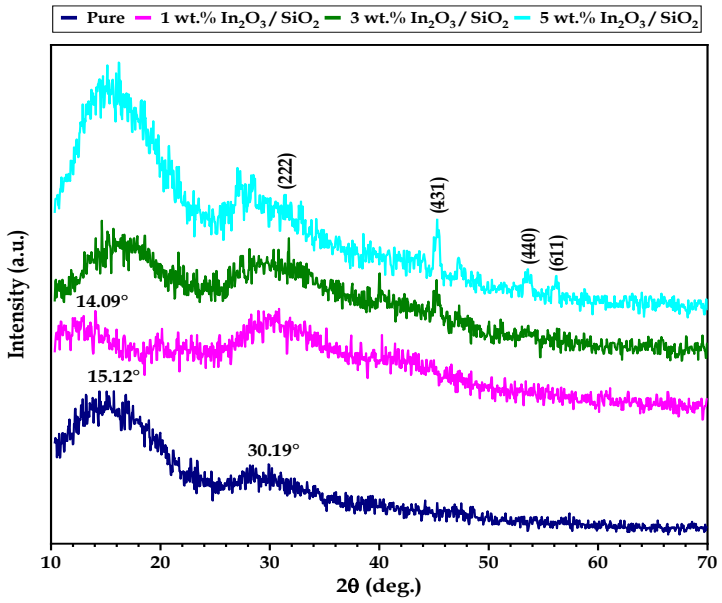

Figure 1 X-ray diffraction for (PMMA/In_2O_3/SiO_2) nanocomposites.

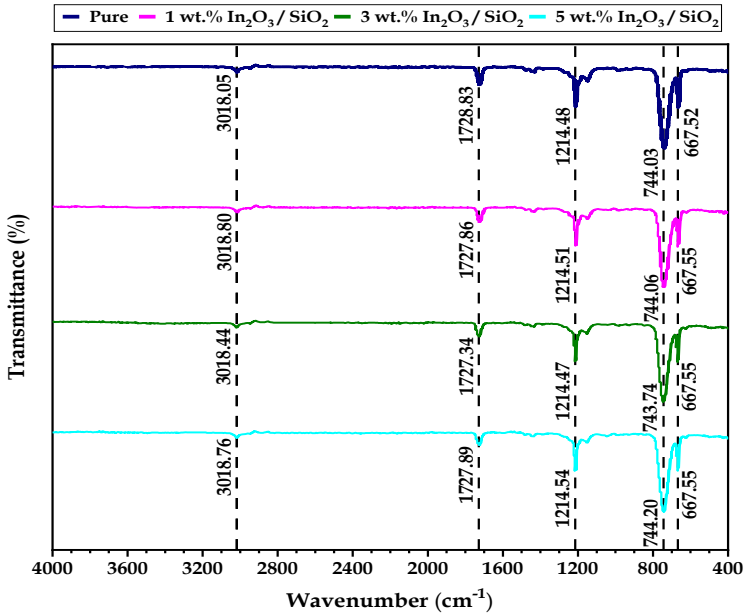

Figure 2 FTIR spectrum for the (PMMA/In_2O_3/SiO_2) nanocomposites:(A) for (PMMA) pure, (B) for 1 wt.% In_2O_3/SiO_2 NPs, (C) for 3 wt.% In_2O_3/SiO_2NPs, (D) for 5wt.% In_2O_3/SiO_2NPs.

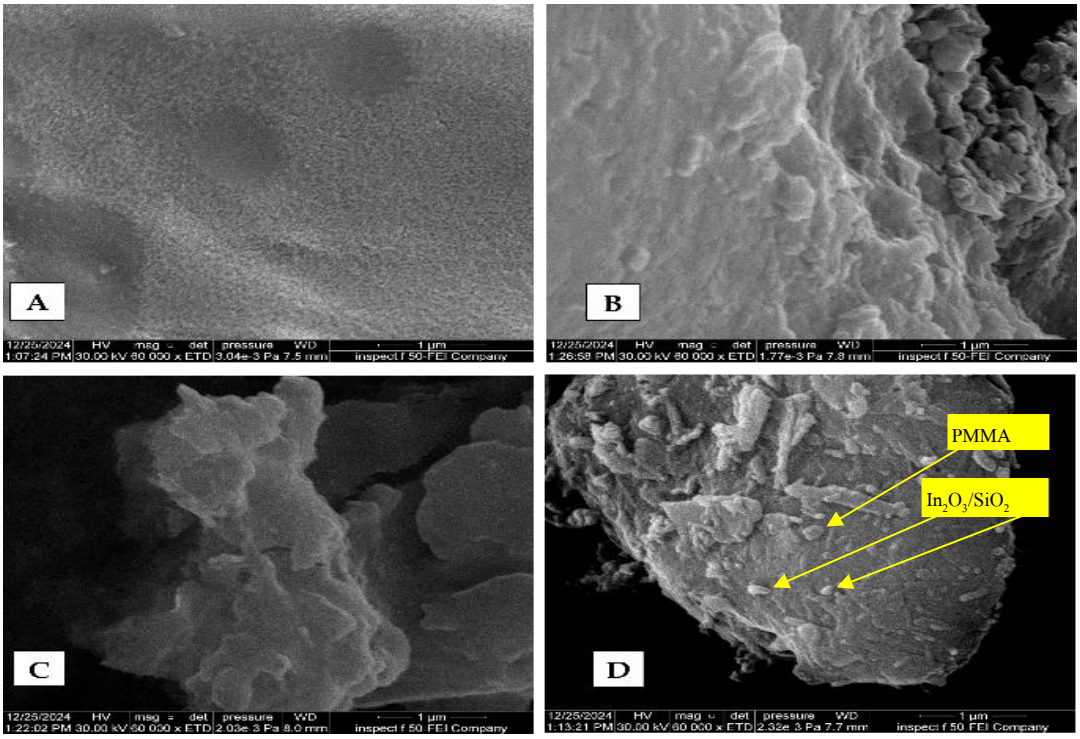

Figure 3 FESEM for the (PMMA/In_2O_3/SiO_2) nanocomposites: (A) for (PMMA) pure, (B) for 1 wt.% In_2O_3/SiO_2 NPs, (C) for 3 wt.% In_2O_3/SiO_2NPs, (D) for 5wt.% In_2O_3/SiO_2NPs.

Figure 4 illustrates the optical absorbance characteristics of pure PMMA and PMMA/In_2O_3/SiO_2 nanocomposites across the wavelength spectrum of 200–800 nm, evaluated in film form. The data indicate that all nanocomposite samples exhibit higher UV absorbance than pure PMMA. The donor material facilitates electron migration into the conduction band at higher energy levels, particularly at a wavelength of 200 nm. This occurs when electrons transition from a lower to a higher energy level upon absorbing a photon of specific energy. The absorbance increases as the concentration of In_2O_3 and SiO_2 nanoparticles rises from 0 wt.% into 5 wt.%. This effect is attributed to the insufficient energy of incoming photons at longer wavelengths, which limits their interaction with atoms and allows them to pass through without significant absorption. The findings align with the current literature [35,36]. The selective absorption of gamma radiation is essential in medical and nuclear industry applications, and the absorption characteristics of PMMA composites can be improved to achieve this. Typically, the mass attenuation coefficient, which is contingent upon the energy of the incident rays and the composite's composition, is employed to determine the attenuation efficacy. The transparency of PMMA composites is essential for the transmission of light. PMMA composites with minimal absorbance are preferred for applications such as optical waveguides, displays, and lenses. The composite's absorption of light may result in energy loss or light dispersal, which is not desirable in numerous devices.

The transmittance (T) given by the relation [37]:

$$T = exp(-2.303\ A) \quad (1)$$

In this context, α represents the absorption coefficient, while t denotes the thickness of the film. **Figure 5** presents the transmittance (T) spectra of PMMA/In_2O_3/SiO_2 nanocomposites across a range of wavelengths. The figure shows a significant increase in transmittance with increasing wavelength, particularly 300 nm. Beyond this point, the transmittance exhibits a stable and consistent increase. The data clearly demonstrate that the incorporation of In_2O_3 and SiO_2 nanoparticles leads to a reduction in light transmittance. This modification enhances the optical properties of the PMMA polymer matrix, resulting in increased light absorption and a corresponding decrease in

transmittance due to the presence of nanomaterials. The transmission of the PMMA/In_2O_3/SiO_2 nanocomposite is contingent upon the extent to which the In_2O_3/SiO_2 nanoparticles are dispersed within the PMMA. Transmittance is diminished as a result of light scattering, which is caused by inadequate dispersion. Additionally, the transmittance is generally reduced by a higher In_2O_3/SiO_2 concentration as a result of increased scattering and absorption. The composite's optical clarity is maintained by its high transmittance, which is advantageous for optical coatings, displays, and lenses. Absorption or scattering, which are frequently associated with material defects or improper dispersion, are indicated by a decrease in transmittance. Composites that exhibit high transmittance and excellent conductivity are optimal for applications such as smart windows and flexible electronics. These findings align with previous research [38].

The absorption coefficient was calculated using an empirical correlation [38].

$$\alpha = 2.303\ A/t \quad (2)$$

The variable A represents the absorbance of the incident photons on the nanocomposite**. Figure 6** illustrates the relationship between absorption coefficient (α) of PMMA/In_2O_3/SiO_2 nanocomposite films and photon energy coefficient exhibits a steady increase with rising photon energy, ultimately reaching a value of 4.14 eV. When the energy of an incoming photon is insufficient to excite an electron from the valence band to the conduction band, the electron transitions to a lower state. At an energy level of 4.14 eV, a significant enhancement in the absorption coefficient is observed across all samples. This process induces notable changes within the conduction band. A higher α is good when absorption is required for UV shielding, photodetectors, optical filters, and radiation attenuation applications. The absorption value remains below 10^4 cm^{-1}, indicating that an indirect transition has occurred [39].

The energy gap is given by [40]:

$$(\alpha h\upsilon)^{1/m} = C(h\upsilon - E_g) \quad (3)$$

Constant C, photon energy $h\upsilon$, energy gap E_g, and the allowed and forbidden indirect transitions m = 2 and 3. To evaluate the band gap energy (E_g), a graph must be plotted relating the product of the absorption coefficient ($\alpha h\upsilon$) and the photon energy ($h\upsilon$) must be constructed. The value of (r) in this calculation is 1/2 if electron transport is allowed, or (1/3) if it is restricted. By extrapolating the linear equations to the $h\upsilon$-axis, the optical band gap values are determined, as shown in **Table 2**. **Figures 7** and **8** illustrate the indirect band of pure PMMA and the PMMA/In_2O_3/SiO_2 nanocomposite. The data indicate that the band gap energy (E_9) decreases as the concentration of In_2O_3/SiO_2 nanoparticles increases. The permissible indirect energy gap decreases from 4.72 to 3.29 eV, while the forbidden indirect energy has declined from 4.37 to 2.65 eV. This phenomenon is attributed to the presence of localized states arising from different within the mobility gap accounts for this result. This result is consistent with previous studies [41,42].

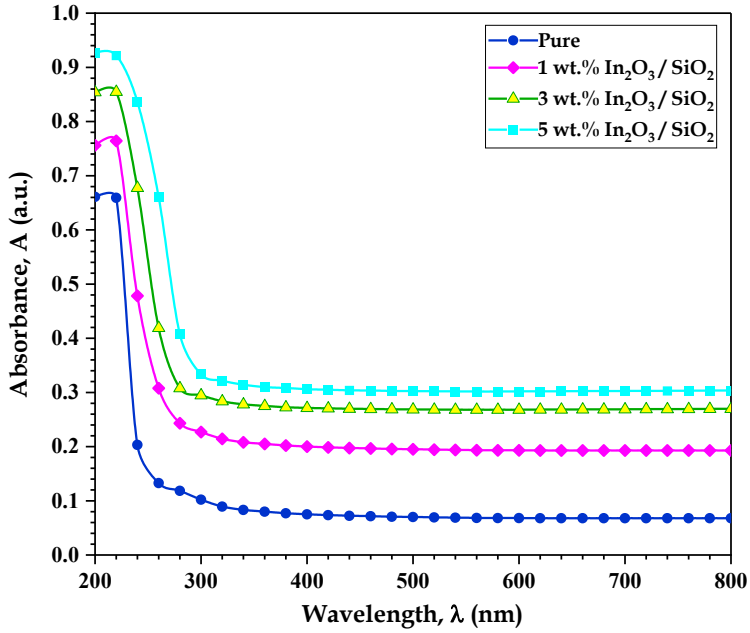

Figure 4 the absorbance of PMMA/In_2O_3/SiO_2 nanocomposite with wavelength.

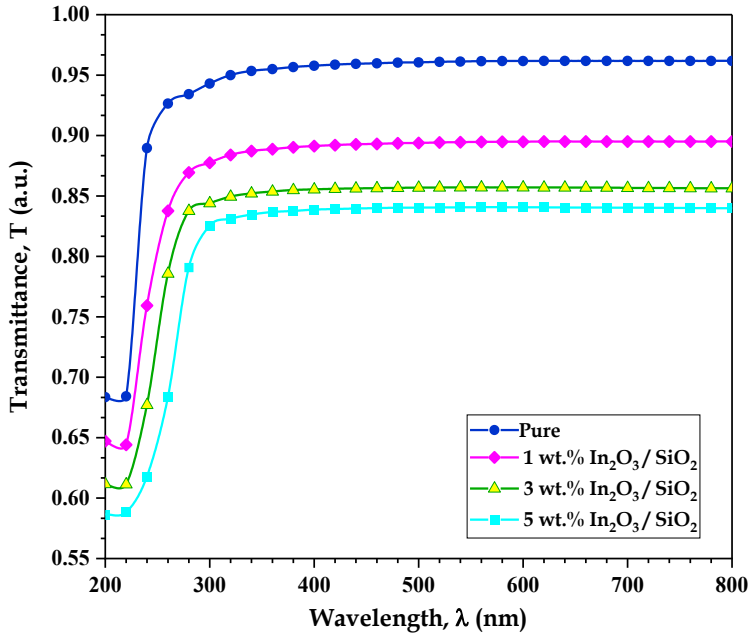

Figure 5 The transmittance of PMMA/In_2O_3/SiO_2 nanocomposite with wavelength.

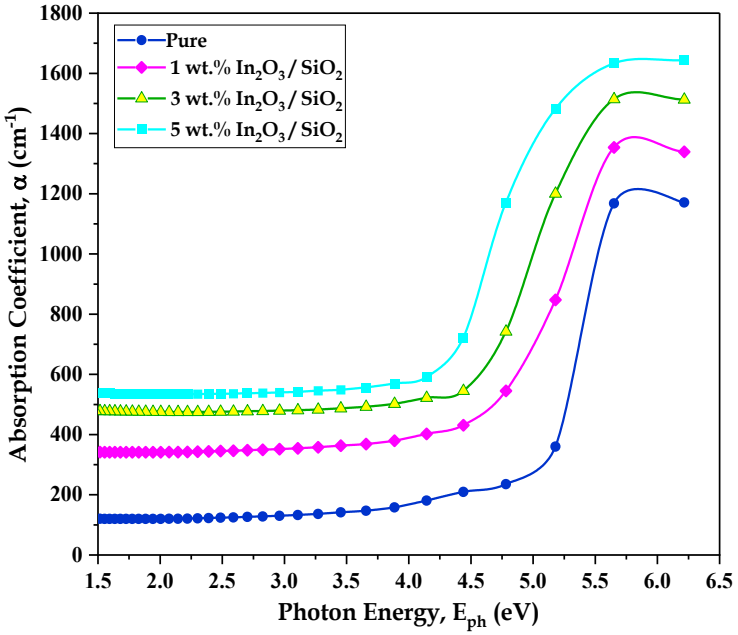

Figure 6 The absorption coefficient of PMMA/In_2O_3/SiO_2 nanocomposite with wavelength.

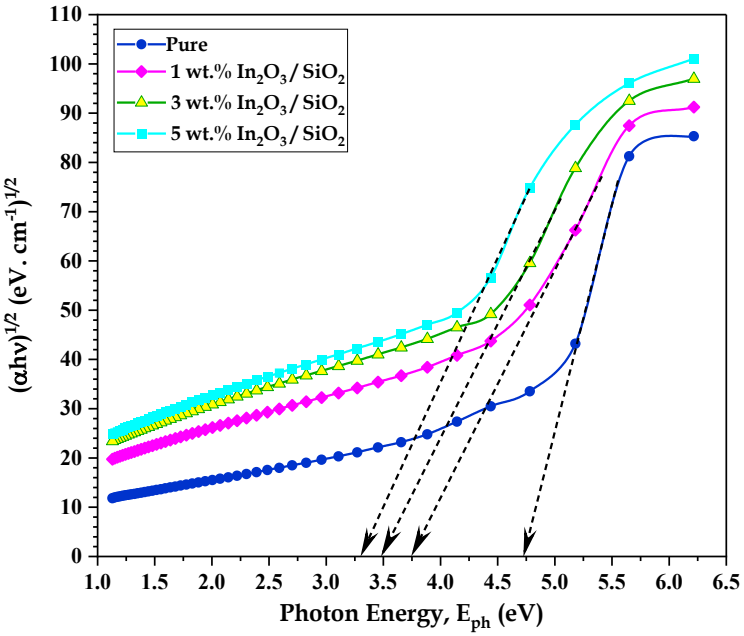

Figure 7 Relation between $(\alpha h\nu)^{1/2}$ versus $(h\nu)$ PMMA/In_2O_3/SiO_2 nanocomposites.

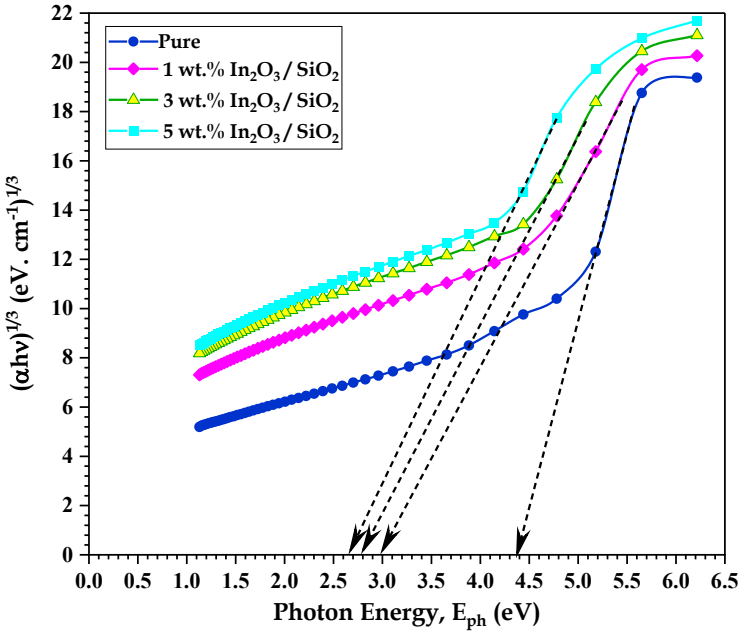

Figure 8 Relation between $(\alpha h\nu)^{1/3}$ versus $(h\nu)$ for PMMA/In_2O_3/SiO_2 nanocomposites.

Table 2 Values of the allowed and forbidden energy gap at the optimum value of PMMA/In_2O_3/SiO_2 nanocomposites.

In_2O_3/SiO_2 (wt.%)	Allowed E_g (eV)	Forbidden E_g (eV)
0	4.72	4.37
1	3.74	2.97
3	3.48	2.77
5	3.29	2.65

The refractive index (n) was determined using the following relation [43]:

$$n = \frac{1+\sqrt{R}}{1-\sqrt{R}} \quad (4)$$

where R denotes the reflectance, **Figure 9** illustrates the refractive index of PMMA/In_2O_3/SiO_2 nanocomposites as a function of wavelength. The incorporation of In_2O_3 and SiO_2 into the polymer matrix results in an increase in the refractive index of the samples. This interaction establishes a linkage between the electrons and the oscillating electromagnetic field. As the concentration of In_2O_3 and SiO_2 nanoparticles increases, the refractive index values correspondingly rise. This behaviour is consistent with the findings of previous studies [44].

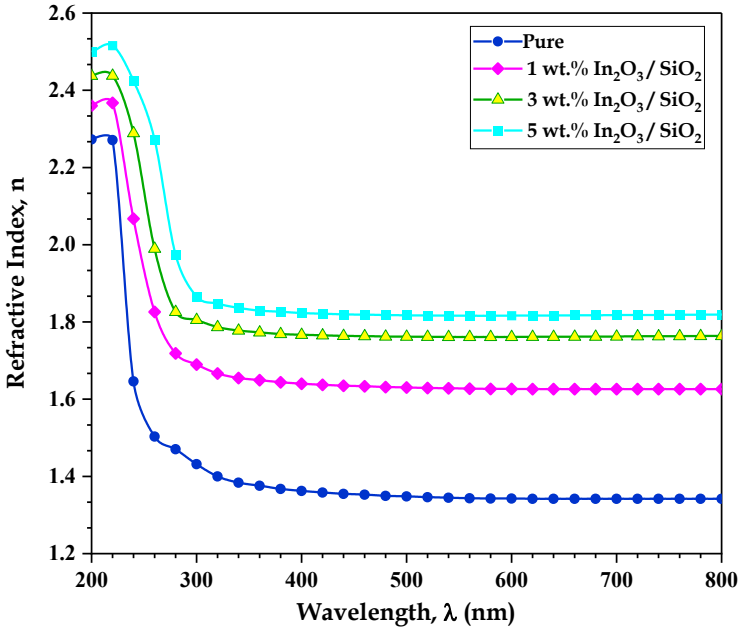

Figure 9 The refractive index of PMMA/In_2O_3/SiO_2 nanocomposite with wavelength.

The extinction coefficient (k) is defined by the Eq. [45]:

$$k = \alpha\lambda/4\pi \quad (5)$$

where the wavelength is denoted by λ.

For all films that were produced, **Figure 10** illustrates the extinction coefficient plotted against frequency. The extinction coefficient of PMMA/In_2O_3/SiO_2 nanocomposites exhibits a substantial increase at lower energies, particularly at 240 nm, followed by a decrease at 320 nm. After 320 nm, the absorption coefficient increased steadily with the addition of In_2O_3 and SiO_2 nanoparticles. The concurrent rise in photon energy could clarify this phenomenon. It is clearly shown that the extinction coefficient of nanocomposites is correlated with the concentration ratio of In_2O_3 and SiO_2 nanoparticles. The explanation for this phenomena is that there is an increase in the amount of light that is absorbed coming in [46].

There are 2 components to the dielectric constant: the real component (ε_1) and the imaginary component (ε_2) [47]:

$$\varepsilon_1 = n^2 - k^2 \quad (6)$$

$$\varepsilon_2 = 2nk \quad (7)$$

Variations in the dielectric constant's real component (ε_1) and imaginary component (ε_2) for PMMA/In_2O_3/SiO_2 nanocomposites are depicted in **Figures 11** and **12**. According to the results, the real and imaginary components of the dielectric constant of pure PMMA polymer are higher at shorter wavelengths but decrease with increasing wavelength. The nanocomposite films exhibit a significant increase in both real and imaginary values as the wavelength decreases, subsequently followed by a considerable decline at high energy levels. The magnitudes of (n) mainly influence the effective dielectric constant because the later values (k) are much lower than the refractive index, particularly when squared [48].

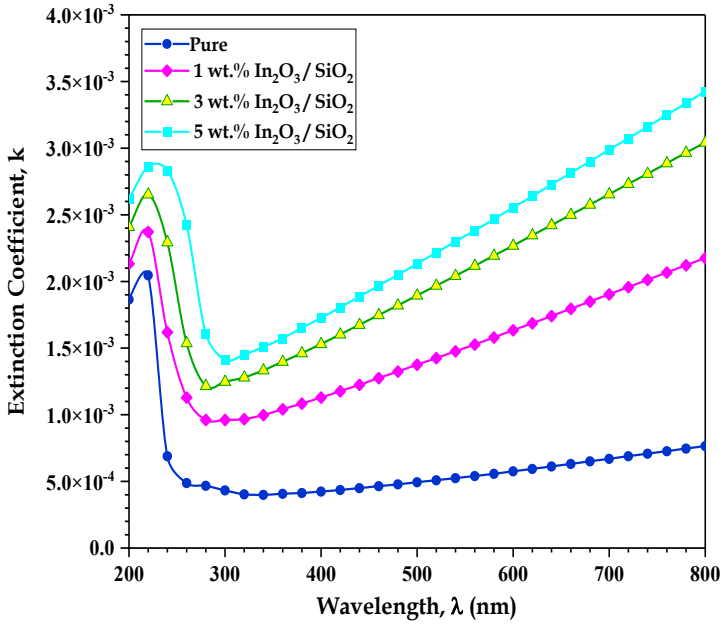

Figure 10 Extinction coefficient of PMMA/In_2O_3/SiO_2 nanocomposites.

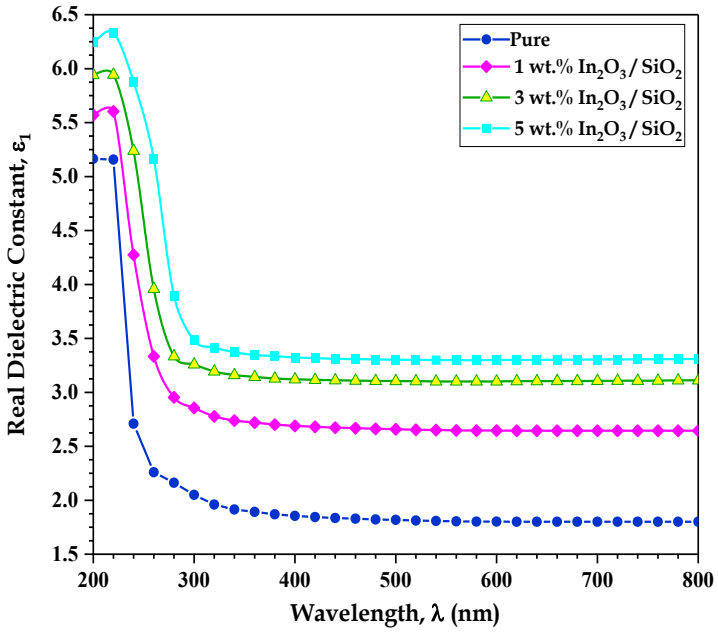

Figure 11 Real dielectric constant of PMMA/In_2O_3/SiO_2 nanocomposites.

The optical conductivity (σ_{op}) is definite by [49]:

$$\sigma_{op} = \alpha nc/4\pi \quad (8)$$

Where c represents the speed of light. **Figure 13** illustrates the optical conductivity of the PMMA/In_2O_3/SiO_2 nanocomposites. In the case of pure PMMA, optical conductivity increases at shorter wavelengths and decreases at longer wavelengths. This behaviour corresponds to a simultaneous rise in the absorption index. The measured optical conductivity exhibits a clear correlation with the concentration of In_2O_3 and SiO_2 nanoparticles. These observations can be attributed to the increase in the absorption [50,51].

Figure 14 presents the variations in (N/N_0) corresponding to different concentrations of In_2O_3 and SiO_2 nanoparticles within the PMMA polymer. The reduction in transmission radiation as the concentrations

of In_2O_3 and SiO_2 nanoparticles rise can be elucidated by an enhancement in attenuation radiation. **Figure 15** demonstrates the effect of the In_2O_3/SiO_2 concentration ratio on changes in gamma attenuation coefficients. As the nanoparticle concentration increases, the attenuation coefficients also rise, since the shielding in nanocomposite either absorb or reflect gamma radiation The high atomic numbers of In_2O_3 and SiO_2 contribute to the highest attenuation coefficients observed in PMMA/In_2O_3/SiO_2 nanostructures [52,53].

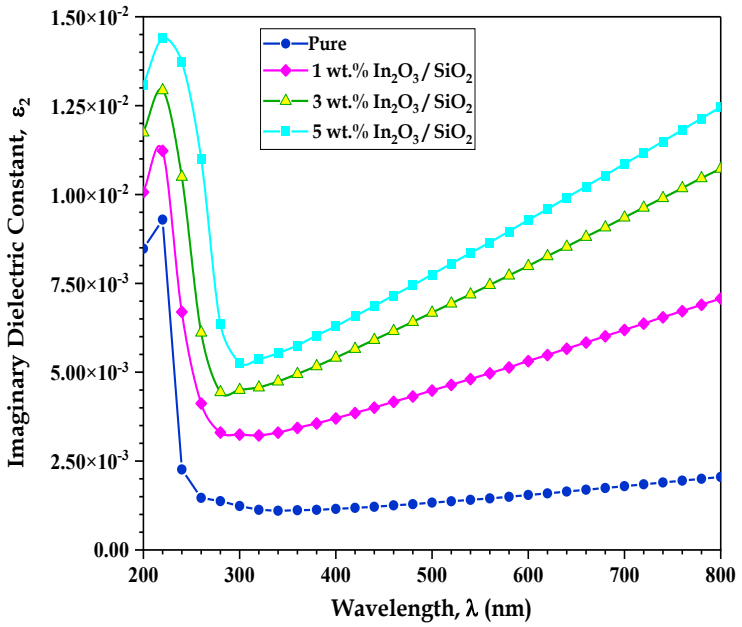

Figure 12 Imaginary dielectric constant of PMMA/In_2O_3/SiO_2 nanocomposites.

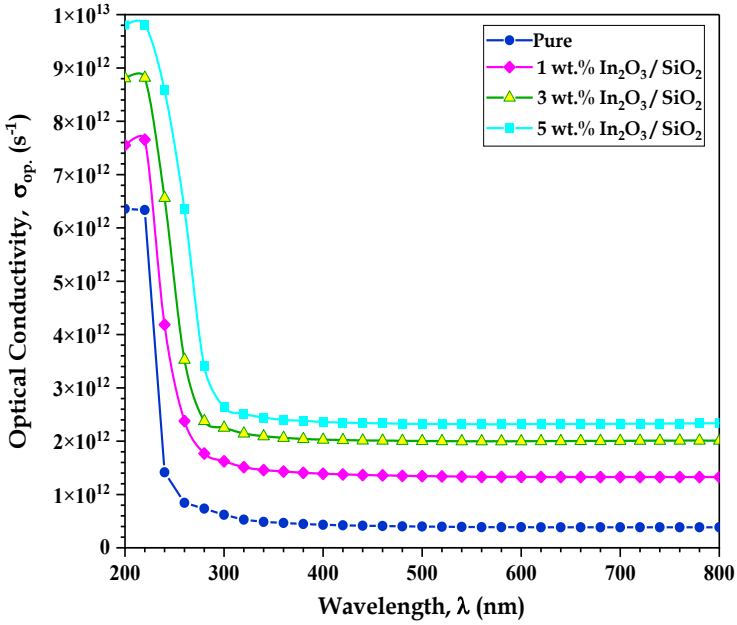

Figure 13 Optical conductivity of PMMA/In_2O_3/SiO_2 nanocomposites.

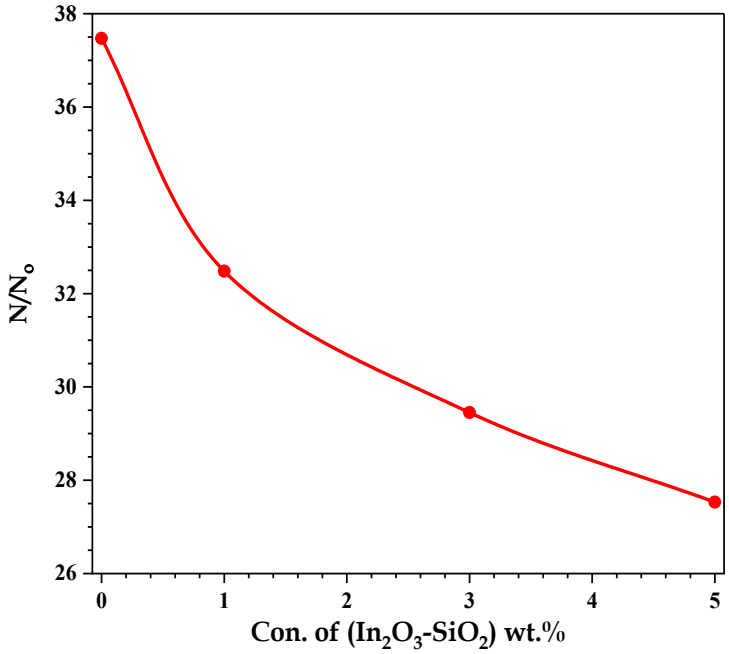

Figure 14 Variation of (N/N_0) for ($PMMA/In_2O_3/SiO_2$) nanostructures.

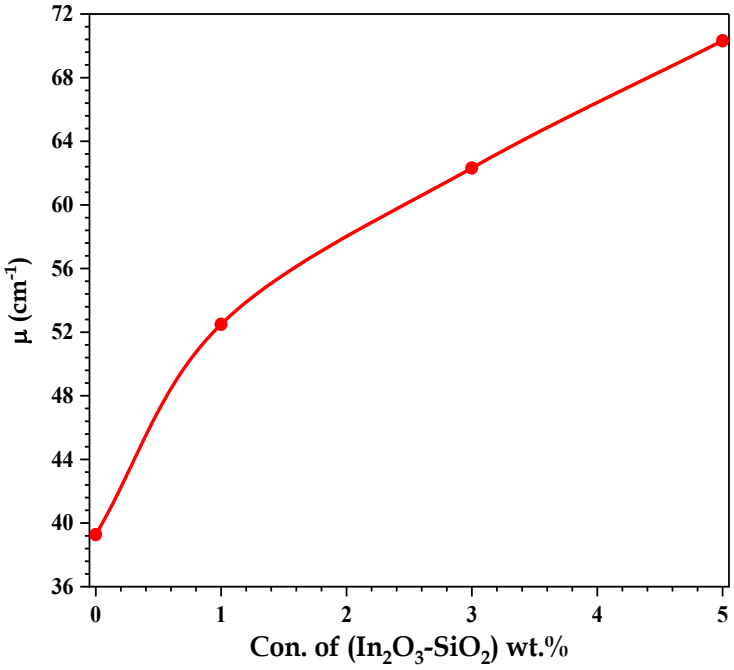

Figure 15 Variation of attenuation coefficients of gamma radiation for ($PMMA/In_2O_3/SiO_2$) nanostructures.

Conclusions

This work presents a summary of an effective casting process for the preparation of $PMMA/In_2O_3/SiO_2$ nanocomposites. The XRD analysis revealed that pure PMMA exhibited an amorphous character, which transformed into a polycrystalline structure upon the incorporation of high-load additives (5 wt.%) of In_2O_3 and SiO_2 nanoparticles. FTIR spectroscopy confirmed the existence of interaction between In_2O_3/SiO_2 nanoparticles and the PMMA polymer matrix. FESEM analysis showed that the nanoparticles were uniformly distributed throughout the

PMMA polymer matrix. compared to similar polymer-based composites, this structural modification suggests better material performance for high-end applications. The optical characteristics demonstrated that an increasing concentration of In_2O_3/SiO_2 nanoparticles in PMMA led to enhancements in the real and energy band gaps, absorption coefficient, refractive index, and extinction coefficient. Conversely, transmittance and the indirect energy gap decreased. Due to these properties, PMMA/In_2O_3/SiO_2 nanostructures exhibit potential for optical and electrical applications. Compared to PMMA composites with other fillers (e.g., ZnO, TiO_2), this research demonstrates a better balance between optical transparency and refractive index, which is crucial for optoelectronic applications. Additionally, the gamma radiation attenuation coefficients increased with higher nanoparticle concentrations, indicating that PMMA/In_2O_3/SiO_2 nanostructures possess significant shielding capabilities. The In_2O_3/SiO_2 nano-system presents an optimal balance between radiation protection, optical performance, and mechanical flexibility when contrasted with comparable polymer nanocomposites (e.g., PMMA/Bi_2O_3, PMMA/ZnO).

Acknowledgements

The authors would like to express their appreciation and thanks to the anonymous editor(s) and reviewers of the journal. In addition, the authors thanks Babylon University, Iraq, for their support.

References

[1] DN Qader, MK Haridharan, G Murali, SR Abid, P Kathirvel, A Mugahed, R Fediuk and AM Onaizi. Experimental investigation of a sustainable reinforced cantilever concrete slab exposed to different intensity of temperatures. *Journal of Materials Research and Technology* 2023; **23**, 2371-2388.

[2] AM Onaizi, M Amran, W Tang, N Betoush, M Alhassan, RSM Rashid, MF Yasin, KH Bayagoob and SA Onaizi. Radiation-shielding concrete: A review of materials, performance, and the impact of radiation on concrete properties. *Journal of Building Engineering* 2024; **97**, 110800.

[3] F Hussain and M Meteab. Nuclear reaction analyses for green chemistry: Evaluating environmental safety in charged particle interactions. *E3S Web of Conferences* 2025; **614**, 04025.

[4] R Moriche, M Sanchez, A Jimenez-Suarez, SG Prolongo and A Urena. Electrically conductive functionalized-GNP/epoxy based composites: From nanocomposite to multiscale glass fibre composite material. *Composites Part B: Engineering* 2016; **98**, 49-55.

[5] S Doagou-Rad, A Islam and TD Merca. An application-oriented roadmap to select polymeric nanocomposites for advanced applications: A review. *Polymer Composites* 2020; **41**, 1153-1189.

[6] CA Harper and EM Petrie. *Plastics Materials and Processes*. Wiley, New Jersey, 2003.

[7] Q Lyu, P Dai and A Chen. Mechanical strengths and optical properties of translucent concrete manufactured by mortar-extrusion 3D printing with polymethyl methacrylate (PMMA) fibers. *Composites Part B: Engineering* 2024; **268**, 111079.

[8] M Madgule, P Deshmukh, K Perveen, MO Qamar, A Razak and AW Wodajo. Experimental investigation on mechanical properties of novel polymer hybrid composite with reinforcement of banana fiber and sugarcane bagasse powder. *Advances in Mechanical Engineering* 2023; **15(10)**, 1-13.

[9] A Srinivas, CG Sreenivasa and M Mahadev. A review on - Variants in specimen preparation of natural fiber composites. *AIP Conference Proceedings* 2024; **3013**, 20013.

[10] E Tang, G Cheng and X Ma. Preparation of nano-ZnO/PMMA composite particles via grafting of the copolymer onto the surface of zinc oxide nanoparticles. *Powder Technology* 2006; **161(3)**, 209-214.

[11] JP Wagh, RR Malagi and M Madgule. Investigative studies on natural fiber reinforced composites for automotive bumper beam applications. *Journal of Reinforced Plastics and Composites* 2024. https://doi.org/10.1177/07316844241260764.

[12] EA Stefanescu, X Tan, Z Lin, N Bowler and MR Kessler. Multifunctional PMMA-Ceramic

composites as structural dielectrics. *Polymer* 2010; **51(24)**, 5823-5832.

[13] DA Sabur, A Hashim, A Hadi, MA Habeeb, BH Rabee and MK Mohammed. Enhancement of optical properties in In2O3-Doped PVA/peg nanostructured films for optoelectronic applications. *Revue des Composites et des Materiaux Avances* 2023; **33(6)**, 411-417.

[14] N Hayder, A Hashim, MA Habeeb, BH Rabee, AG Hadi and MK Mohammed. Analysis of dielectric properties of PVA/PEG/In_2O_3 nanostructures for electronics devices. *Revue des Composites et des Materiaux Avances* 2022; **32(5)**, 261-264.

[15] MM Bagheri-Mohagheghi, N Shahtahmasebi, E Mozafari and M Shokooh-Saremi. Effect of the synthesis route on the structural properties and shape of the indium oxide (In_2O_3) nano-particles. *Physica E: Low-dimensional Systems and Nanostructures* 2009; **41(10)**, 1757-1762.

[16] ZA Husain, AA Majeed, RT Rasheed, HS Mansoor and NN Hussein. Antibacterial activity of In2O3 nanopowders prepared by hydrothermal method. *Materials Today: Proceedings* 2021; **42(5)**, 1816-1821.

[17] G Liu. Synthesis, characterization of In2O3 nanocrystals and their photoluminescence property. *International Journal of Electrochemical Science* 2011; **6(6)**, 2162-2170.

[18] MH Meteab, A Hashim and BH Rabee. Synthesis and structural properties of (PS–PC/Co_2O_3–SiC) nanocomposites for antibacterial applications. *Nanosistemi, Nanomater Nanotehnologii* 2023; **21(2)**, 451-460.

[19] A Kolmakov, DO Klenov, Y Lilach, S Stemmer and M Moskovits. Enhanced gas sensing by individual SnO_2 nanowires and nanobelts functionalized with Pd catalyst particles. *Nano Letters* 2005; **5(4)**, 667-673.

[20] SG Ghanati, B Dogan and MK Yesilyurt. The effects of the usage of silicon dioxide (SiO_2) and titanium dioxide (TiO_2) as nano-sized fuel additives on the engine characteristics in diesel engines: A review. *Biofuels* 2024; **15(2)**, 229-243.

[21] TS Soliman, SA Vshivkov and SI Elkalashy. Structural, thermal, and linear optical properties of SiO_2 nanoparticles dispersed in polyvinyl alcohol nanocomposite films. *Polymer Composites* 2020; **41(8)**, 3340-3350.

[22] S Mallakpour and Z Khani. Fabrication of poly (vinyl alcohol) nanocomposites having different contents of modified SiO_2 by vitamin B1 as biosafe and novel coupling agent to improve mechanical and thermal properties. *Polymer Composites* 2018; **39(S3)**, E1589-E1597.

[23] TP Nguyen. Polymer-based nanocomposites for organic optoelectronic devices. A review. *Surface and Coatings Technology* 2011; **206(4)**, 742-752.

[24] S Sugumaran, CS Bellan and M Nadimuthu. Characterization of composite PVA–Al_2O_3 thin films prepared by dip coating method. *Iranian Polymer Journal* 2015; **24**, 63-74.

[25] Q Huang, A Ayyaz, MA Farooq, K Zhang, W Chen, F Hannan, Y Sun, K Shahzad, B Ali and W Zhou. Silicon dioxide nanoparticles enhance plant growth, photosynthetic performance, and antioxidants defence machinery through suppressing chromium uptake in Brassica napus L. *Environmental Pollution* 2024; **342**, 123013.

[26] TS Soliman, A Khalid, M Taha and RM Ahmed. Nanocomposite film combines polyvinyl alcohol and iron oxide capped in silica for optical applications. *Optical and Quantum Electronics* 2024; **56**, 786.

[27] S Jabeen, S Gul, A Kausar, B Muhammad, M Nawaz, KM Saud and M Farooq. A facile route for the synthesis of mechanically strong MWCNTs/NDs nanobifiller filled polyacrylate composites. *Polymer-Plastics Technology and Materials* 2019; **58(16)**, 1810-1827.

[28] KN Fatema, S Sagadevan, Y Liu, K Cho, C Jung and W Oh. New design of mesoporous SiO_2 combined In_2O_3-graphene semiconductor nanocomposite for highly effective and selective gas detection. *Polymer-Plastics Technology and Materials* 2020; **55**, 13085-13101.

[29] N Bajpai, A Tiwari, SA Khan, RS Kher, N Bramhe and SJ Dhoble. Effects of rare earth ions (Tb, Ce, Eu, Dy) on the thermoluminescence characteristics of sol–gel derived and γ-irradiated SiO 2 nanoparticles. *Luminescence* 2014; **29(6)**, 669-673.

[30] MO Bensaid, L Ghalouci, S Hiadsi, F Lakhdari, N Benharrats and G Vergoten. Molecular mechanics investigation of some acrylic polymers using SPASIBA force field. *Vibrational Spectroscopy* 2014; **74**, 20-32.

[31] S Ramesh, KH Leen, K Kumutha and AK Arof. FTIR studies of PVC/PMMA blend based polymer electrolytes. *Spectrochimica Acta Part A: Molecular and Biomolecular Spectroscopy* 2007; **66(4-5)**, 1237-1242.

[32] VN Rai, C Mukherjee and B Jain. *Optical properties (uv-vis and ftir) of gamma irradiated polymethyl methacrylate (pmma).* ArXiv, New York, 2016.

[33] D Nayak and RB Choudhary. Augmented optical and electrical properties of PMMA-ZnS nanocomposites as emissive layer for OLED applications. *Optical Materials* 2019; **91**, 470-481.

[34] AA Raffi, MA Rahman, MAM Salim, NJ Ismail, MHD Othman, AF Ismail and H Bakhtiar. Surface treatment on polymeric polymethyl methacrylate (PMMA) core via dip-coating photopolymerisation curing method. *Optical Fiber Technology* 2020; **57**, 102215.

[35] P Phukan and D Saikia. Optical and structural investigation of CdSe quantum dots dispersed in PVA matrix and photovoltaic applications. *International Journal of Photoenergy* 2013; **2013(21)**, 728280.

[36] Q Luo, Y Shan, X Zuo and J Liu. Anisotropic tough poly(vinyl alcohol)/graphene oxide nanocomposite hydrogels for potential biomedical applications. *RSC Advances* 2018; **8(24)**, 13284-13291.

[37] MK Mohammed, G Al-Dahash and A Al-Nafiey. Fabrication and characterization of the PMMA/G/Ag nanocomposite by pulsed laser ablation (PLAL). *Nano Biomedicine and Engineering* 2022; **14(1)**, 15-22.

[38] Mohammed MK, Khudhair TN, Sharba KS, Hashim A, Hadi QM, and Meteab MH. Tuning the morphological and optical characteristics of SnO2/ZrO2 nanomaterials Doped PEO for promising optoelectronics applications. *Revue des Composites des Materiaux Avances* 2024; **34(4)**, 495-503.

[39] AA Jabber and AR Abdulridha. Preparation and characterization of CuO/ZnO nanostructures thin films using thermal evaporation for advanced gas sensing applications. *Trends in Sciences* 2025; **22(3)**, 9002.

[40] HM Zidan, EM Abdelrazek, AM Abdelghany and AE Tarabiah AE. Characterization and some physical studies of PVA/PVP filled with MWCNTs. *Journal of Materials Research and Technology* 2019; **8(1)**, 904-913.

[41] HM Zidan and M Abu-Elnader. Structural and optical properties of pure PMMA and metal chloride-doped PMMA films. *Physica B: Condensed Matter* 2005; **355(1-4)**, 308-317.

[42] A Rahma, MM Munir, Khairurrijal, A Prasetyo, V Suendo and H Rachmawati. Intermolecular Interactions and the release pattern of electrospun curcumin-polyvinyl(pyrrolidone) fiber. *Biological and Pharmaceutical Bulletin* 2016; **39(2)**, 163-173.

[43] TS Soliman. Investigation of structural and optical features of polyvinyl alcohol films doped with Nd2O3 nanoparticles for UV shielding. *Optical and Quantum Electronics* 2024; **56**, 1217.

[44] SS Mousavi, B Sajad and MH Majlesara. Fast response ZnO/PVA nanocomposite-based photodiodes modified by graphene quantum dots. *Materials & Design* 2019; **162**, 249-255.

[45] LK Mireles, M Wu, N Saadeh, L Yahia and E Sacher. Physicochemical characterization of polyvinyl pyrrolidone: A tale of two polyvinyl pyrrolidones. *ACS Omega* 2020; **5(47)**, 30461-30467.

[46] NM Farrage, NH Teleb and WAA El-Ghany. Investigation of the structural and optical properties of Sb_2S_3/PVA/PVP nanocomposites blended sheets for optoelectronic applications. *Optical and Quantum Electronics* 2024; **56**, 488.

[47] J Fal, K Bulanda, J Traciak, J Sobczak, R Kuziola, KM Graz, G Budzik, M Oleksy and G Zyla. Electrical and optical properties of silicon oxide lignin polylactide (SiO_2-L-PLA). *Molecules* 2020; **25(6)**, 1354.

[48] A Badawi, SS Alharthi, MG Althobaiti and AN Alharbi. The effect of iron oxide content on the structural and optical parameters of polyvinyl

alcohol/graphene nanocomposite films. *Journal of Vinyl and Additive Technology* 2022; **28**, 235-246.

[49] AAA Ahmed, AAA Al-Mushki, BA Al-Asbahi, AM Abdulwahab, JMA Abduljalil, FAA Saad, SMH Qaid, HM Ghaithan, WA Farooq and AH Omar. Effect of ethylene glycol concentration on the structural and optical properties of multimetal oxide CdO–NiO–Fe_2O_3 nanocomposites for antibacterial activity. *Journal of Physics and Chemistry of Solids* 2021; **155**, 110113.

[50] K SK, V N, RB B and S Madivalappa. Structural and optical properties of polyvinyl alcohol/copper oxide (PVA/CuO) nanocomposites. *Solid State Communications* 2023; **370**, 115221.

[51] Q Jebur, A Hashim and M Habeeb. Fabrication, Structural and optical properties for (polyvinyl alcohol–polyethylene oxide–iron oxide) nanocomposites. *Egyptian Journal of Chemistry* 2019; **63(2)**, 611-623.

[52] T Saini, J Meena, V Verma, S Saini and R Malik. Polyvinyl alcohol: Recent advances and applications in sustainable materials. *Polymer-Plastics Technology and Materials* 2024; **64(6)**, 794-825.

[53] HH Jassim and FS Hashim. Synthesis of (PVA/PEG: ZnO and Co_3O_4) nanocomposites: Characterization and gamma ray studies. *NeuroQuantology* 2021; **19(4)**, 47.